COMMUNICATIONS IN COMPUTATIONAL PHYSICS
Vol. **3**, No. 1, pp. 203-221

Commun. Comput. Phys.
January 2008

Amplitude Compensation for One-Way Wave Propagators in Inhomogeneous Media and its Application to Seismic Imaging

Jun Cao[1,*] and Ru-Shan Wu[2]

[1] *Department of Earth and Planetary Sciences, University of California, Santa Cruz, CA 95064, USA.*
[2] *CSIDE, Institute of Geophysics and Planetary Physics, University of California, Santa Cruz, CA 95064, USA.*

Received 5 December 2006; Accepted (in revised version) 6 June, 2007

Available online 14 September 2007

Abstract. The WKBJ solution for the one-way wave equations in media with smoothly varying velocity variation with depth, $c(z)$, is reformulated from the principle of energy flux conservation for acoustic media. The formulation is then extended to general heterogeneous media with local angle domain methods by introducing the concepts of Transparent Boundary Condition (TBC) and Transparent Propagator (TP). The influence of the WKBJ correction on image amplitudes in seismic imaging, such as depth migration in exploration seismology, is investigated in both smoothly varying $c(z)$ and general heterogeneous media. We also compare the effect of the propagator amplitude compensation with the effect of the acquisition aperture correction on the image amplitude. Numerical results in a smoothly varying $c(z)$ medium demonstrate that the WKBJ correction significantly improves the one-way wave propagator amplitudes, which, after compensation, agree very well with those from the full wave equation method. Images for a point scatterer in a smoothly varying $c(z)$ medium show that the WKBJ correction has some improvement on the image amplitude, though it is not very significant. The results in a general heterogeneous medium (2D SEG/EAGE salt model) show similar phenomena. When the acquisition aperture correction is applied, the image improves significantly in both the smoothly varying $c(z)$ medium and the 2D SEG/EAGE salt model. The comparisons indicate that although the WKBJ compensation for propagator amplitude may be important for forward modeling (especially for wide-angle waves), its effect on the image amplitude in seismic imaging is much less noticeable compared with the acquisition aperture correction for migration with limited acquisition aperture in general heterogeneous media.

AMS subject classifications: 65T60, 86A15

Key words: Propagator amplitude, image amplitude, WKBJ, beamlet, local angle domain, seismic imaging.

*Corresponding author. *Email addresses:* jcao@pmc.ucsc.edu (J. Cao), wrs@pmc.ucsc.edu (R. S. Wu)

1 Introduction

Full wave equation based modeling methods (e.g., finite-difference, finite-element) can model all wave phenomena and provide accurate amplitudes of the wavefield, but are computationally expensive, especially for the 3D case. Asymptotic theory based methods, such as the ray method, have been widely used in industry due to their efficiency, straightforward implementation and flexibility in target-oriented imaging. The high-frequency approximation limits their application in complicated regions. One-way wave equation (parabolic wave equation) based propagators provide powerful and fast tools for forward modeling and migration. They are much faster than full wave methods and can handle complex velocity models better than ray-based methods. The original one-way wave equations, introduced to exploration geophysics by Claerbout [1, 2], do not provide accurate amplitudes even at the level of leading order asymptotic WKBJ or ray-theoretical amplitudes [3].

The conventional one-way wave equation based migration can offer reflector maps consistent with real subsurface structures, but may provide unreliable reflection/scattering strength (or image amplitude) of the reflectors/scattering objects. True-reflection (or true-amplitude) imaging tries to give not only correct location but also correct image amplitude of the reflectors. This can bridge the gap between the conventional imaging and direct inversion of the medium parameters. There are many factors which may influence the image amplitude, including propagator errors (e.g., focusing and defocusing by heterogeneity, geometrical spreading, path absorption and path scattering loss, numerical dispersion and numerical anisotropy), acquisition aperture effects, imaging conditions, etc.

The amplitude errors in the conventional one-way wave propagators have been studied by different approaches for a long time [3–10]. The WKBJ correction can be introduced into the one-way wave equations to compensate the amplitude of the propagators. Traditionally, the WKBJ solution is derived by asymptotic approximation in smoothly varying $c(z)$ media [11–14]. It has also been obtained by approximately factorizing the full-wave operator into one-way wave operators in heterogeneous media [4]. With an extra amplitude term introduced to the conventional one-way wave equations, the first-order transport equation of the one-way wave equation will be the same as that from the full-wave equation in the sense of high-frequency approximation. In this sense, they are called "true-amplitude" one-way wave equations [3].

Understanding the reciprocity properties of (forward and inverse) one-way propagators is relevant for the design of true-amplitude migration schemes [7]. The usual one-way propagators are pressure-normalized: the sum of the downgoing and upgoing waves equals the acoustic pressure of the total wavefield, and they do not obey reciprocity [7]. The so called flux-normalized [5–7,15–17] one-way propagators, in which the transmission coefficients at an interface for downgoing and upgoing waves are identical, on the other hand, do obey reciprocity [7]. For horizontally layered media there is a vast amount of literature that makes use of the flux-normalized decomposition [15–17]. It can

be generalized for applications in arbitrarily inhomogeneous media [5, 6].

Recently, a multi-one-way method [8] has been proposed to improve the estimation of amplitudes in conventional one-way propagators. It is based on an iterative solution of the factorized full wave equation with a right-hand side incorporating the information about medium heterogeneities using the perturbation theory, which assumes small velocity contrasts. This approach takes into account vertical and horizontal velocity variations of the medium and allows modeling of reflected waves. The scheme consists of a succession of several classic one-way wave propagations, but with a right-hand side that is constructed from the error (correction) operator. These make it five times more computationally expensive than the classic one-way scheme. Numerical results for several 2D examples with smoothly varying and rough velocity contrasts show that this scheme significantly reduces the error in the amplitude estimates of the wavefield when compared with the conventional one-way propagators.

With the WKBJ corrected "true-amplitude" one-way wave equations, better image amplitude is obtained in common-shot migration in some smoothly varying models [3, 18]. Based on the multi-one-way modeling method, a true-amplitude multi-one-way migration method is proposed to retrieve the true reflectivity [19], which is based on a small reflection angle hypothesis.

The limited data acquisition aperture in reality combined with complex overburden structures often results in strongly non-uniform dip-dependant illumination of some subsurface structures. Wu et al. [20] proposed an amplitude correction method in local angle domain for acquisition aperture correction. Numerical examples showed significant improvement in both the total strength of the images and angle-dependent reflection amplitudes. This demonstrated the significance of aperture correction in true-reflection imaging.

Different from the ray-based methods, usually there is no local angle information in wave equation based migration methods. Recently developed methods, such as local plane wave analysis based on window Fourier Frame theory [21, 22] or local slant stack [23, 24], can decompose the wavefield into localized beamlets bearing angle information, which make it possible to form images in the local angle domain.

Most amplitude compensation schemes of one-way propagators are formulated and implemented in the space domain. The localized WKBJ correction for general heterogeneous media proposed in [9] is in the local angle (wavenumber) domain. For general heterogeneous media, the global wavenumber does not have the same meaning as for laterally homogeneous media and cannot be related to the propagation direction of local plane waves. The beamlet method [25], which contains localized wavenumber and location information, could be used to implement the localized WKBJ correction [10].

In this paper, the WKBJ solution is reformulated from the conservation of energy flux in smoothly varying $c(z)$ media and then extended to general heterogeneous media in the local angle domain using a beamlet propagator. The imaging condition in the space and space-local angle domain and the formula for the acquisition aperture correction are then given. In the numerical examples, the one-way wave amplitudes before and after the

WKBJ correction are compared with the results from the full-wave method in a smoothly varying $c(z)$ medium. Finally we apply the WKBJ-corrected one-way propagator to the seismic imaging (depth migration) and compare the influence of the propagator amplitude correction with that of the acquisition aperture correction on the image amplitude in both the smoothly varying $c(z)$ and general heterogeneous media.

2 Amplitude WKBJ compensation for the conventional one-way propagator

2.1 WKBJ solution from energy flux conservation in smoothly varying $c(z)$ media

The WKBJ solution can be derived from energy flux conservation. Energy flux rate is the amount of energy transmitted per unit time across unit area normal to the direction of propagation [12]. In general elastic media, the strain energy density is

$$\frac{1}{2}\boldsymbol{\tau}:\boldsymbol{\varepsilon}=\frac{1}{2}\sum_{i,j}\tau_{ij}\varepsilon_{ij}, \tag{2.1}$$

where $\boldsymbol{\tau}$,$\boldsymbol{\varepsilon}$ is the stress and strain tensor. It can be shown that for plane waves the strain energy equals the kinetic energy. In the case of acoustic media, the kinetic energy density of plane waves is $\frac{1}{2}\rho\dot{u}^2$, where ρ,u and $\dot{u}=v$ are media density, particle displacement and particle velocity, respectively. This means, for plane waves, energy flux rate is ρcv^2, where c is the wave propagation speed.

For acoustic media, Newton's Law in the frequency domain is

$$-\nabla P=-i\omega\rho\vec{v}. \tag{2.2}$$

For the vertical direction, we have

$$\frac{\partial P}{\partial z}=i\omega\rho v_z, \tag{2.3}$$

$$v_z=\frac{1}{i\omega\rho}\frac{\partial P}{\partial z}. \tag{2.4}$$

For the plane wave pressure field

$$P=P_0\exp[i(k_x x+k_z z-\omega t)], \tag{2.5}$$

we have

$$\frac{\partial P}{\partial z}=ik_z P=ik_0\cos\theta_i P, \tag{2.6}$$

where $k_0=\omega/c$; θ_i is the propagation angle with respect to the vertical direction (see Fig. 1). Substituting (2.6) into (2.4), we have

$$P=\frac{\rho cv_z}{\cos\theta_i}=\rho cv. \tag{2.7}$$

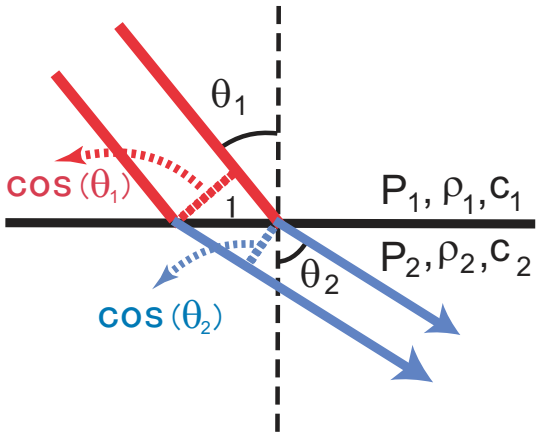

Figure 1: Diagram showing the wave propagation and energy flux conservation across the boundary of a two-layered medium.

With (2.7), we can get the energy flux incident on a unit area of the horizontal interface per unit time (see Fig. 1)

$$\rho c v^2 \cos\theta_i = \frac{P^2 \cos\theta_i}{\rho c}.$$

For laterally homogeneous media, the energy flux conservation (see Fig. 1) leads to

$$\frac{P_1^2 \cos\theta_1}{\rho_1 c_1} = \frac{P_2^2 \cos\theta_2}{\rho_2 c_2}. \tag{2.8}$$

We can recognize that $\rho_1 c_1 / \cos\theta_1 = Z_1$ is the local impedance of the media to a plane wave with propagation angle θ_1. From (2.8) we can get the pressure field change along the z-direction across the media boundary

$$\frac{P_2}{P_1} = \sqrt{\frac{\cos\theta_1}{\cos\theta_2}\frac{\rho_2 c_2}{\rho_1 c_1}} = \sqrt{\frac{\rho_2}{\rho_1}}\sqrt{\frac{k_z(c_1)}{k_z(c_2)}}. \tag{2.9}$$

Eq. (2.9) agrees with the WKBJ solution for smoothly varying media (e.g., in [14]).

2.2 WKBJ solution extended to general heterogeneous media

The amplitude of the conventional one-way propagators can be compensated by using either the transmission coefficient correction or the WKBJ correction. The former correction can give the correct amplitude of the wavefield by taking into account the loss of reflected energy during propagation in non-smoothly varying media. For the WKBJ correction, there is no energy loss during propagation due to the smoothly varying media assumption. We can generalize the WKBJ solution for smoothly varying $c(z)$ media to

a transparent (or energy-conservative) propagator for general $c(z)$ media. For $c(z)$ media with discontinuities, the solution (2.9) corresponds to a TBC at each interface and the propagator becomes a TP, which neglects all of the scattered/reflected energy loss when the waves cross the boundary. The energy flow is thus continuous and conserved in both the smoothly varying media and the media with sharp boundaries. Although the TBC for the media with discontinuities does not represent physical reality, it could be useful and preferred for some inversion procedures or true-reflection imaging because we can conserve all of the energy collected by the receiver array. This could be the best strategy for imaging, since we do not want to lose any more energy from the already weak signals [20].

Along this line, the concept of TP of the wavefield can be extended to general heterogeneous media in the local angle domain [9], which can be called the localized WKBJ correction. The concept of the TP is similar to the flux-normalized propagator for general heterogeneous media. It can be implemented using a Local Cosine Basis (LCB) beamlet propagator [10]. Here we give a summary of the theory. At each depth level, the space-domain wavefield for a given frequency can be decomposed into beamlets as [25]

$$u(x,z,\omega)=\sum_n\sum_m u(\bar{x}_n,\bar{\xi}_m,z,\omega)\cdot b_{mn}(x), \tag{2.10}$$

where b_{mn} is the decomposition basis vector (beamlet) and $u(\bar{x}_n,\bar{\xi}_m)$ is the coefficient of the decomposed beamlet. The basis element b_{mn} can be characterized by the window position $\bar{x}_n$, window interval (the nominal length of the window) $L_n=\bar{x}_{n+1}-\bar{x}_n$, and wavenumber $\bar{\xi}_m$ as follows

$$\begin{aligned} b_{mn}(x)&=\sqrt{\frac{2}{L_n}}B_n(x)\cos\left(\bar{\xi}_m(x-\bar{x}_n)\right),\\ \bar{\xi}_m&=\frac{\pi\left(m+\frac{1}{2}\right)}{L_n}, \end{aligned} \tag{2.11}$$

where $B_n(x)$ is a smooth bell (window) function.

According to the global WKBJ correction in smoothly varying $c(z)$ media (2.9), the localized WKBJ correction in general heterogeneous media based on the beamlet propagator can be symbolically written as

$$\frac{u(\bar{x}_n,\bar{\xi}_m,z+\Delta z,\omega)}{u(\bar{x}_n,\bar{\xi}_m,z,\omega)}=\sqrt{\frac{\rho(\bar{x}_n,z+\Delta z)}{\rho(\bar{x}_n,z)}}\sqrt{\frac{k_z(\bar{x}_n,z)}{k_z(\bar{x}_n,z+\Delta z)}}, \tag{2.12}$$

$$k_z^2(\bar{x}_n,z)=\omega^2/v^2(\bar{x}_n,z)-\bar{\xi}_m^2, \tag{2.13}$$

where $k_z(\bar{x}_n,z)$ is the window-position dependent local vertical wavenumber at depth z, and $v(\bar{x}_n,z)$ is the reference velocity for window at $\bar{x}_n$. In comparison, the vertical wavenumber, $k_z(z)$, in (2.5) and the reference velocity are lateral-position independent for the global WKBJ correction (2.9) in the laterally homogeneous media.

3 Imaging condition in the space and space-local angle domain

Since we implement the one-way propagator in the frequency domain here, we focus on the imaging condition in the frequency domain only. In common shot migration, the source wavefield for each shot is forward-propagated, and the corresponding recorded data are back-propagated to the imaging space. At each depth, the conventional space-domain imaging condition for single frequency [26] can be used to construct the single-shot image, and the final image is obtained by summing up all of the single-shot images together

$$I(\mathbf{x})=\sum_{\mathbf{x}_s} I(\mathbf{x};\mathbf{x}_s)=\sum_{\mathbf{x}_s} 2G_I^*(\mathbf{x};\mathbf{x}_s)\cdot\int_{A(\mathbf{x}_g)} d\mathbf{x}_g \frac{\partial G_I^*(\mathbf{x};\mathbf{x}_g)}{\partial z} u_s(\mathbf{x}_g;\mathbf{x}_s), \tag{3.1}$$

where $I(\mathbf{x};\mathbf{x}_s)$ is the single-shot image from the shot at $\mathbf{x}_s$; G_I is the Green's function used in the imaging process, which could be different from the Green's function used in the forward modeling; "*" stands for complex conjugate; and the integral is a back propagation Rayleigh integral of the recorded data, in which $A(\mathbf{x}_g)$ is the spatial receiver aperture and $u_s(\mathbf{x}_g;\mathbf{x}_s)$ is the recorded scattered wavefield at the receiver $\mathbf{x}_g$ from the source at $\mathbf{x}_s$.

Seismic imaging should provide us an estimate of the subsurface reflectivity/scattering strength, which is reflection/scattering angle dependent. Therefore the imaging condition in the space domain (3.1) needs to be extended to the space-local angle domain (or beamlet domain) [21,27]. Then the image obtained at each imaging point is no longer a scalar value but a matrix, called the local image matrix (LIM) $L(\bar{\mathbf{x}},\bar{\theta}_s,\bar{\theta}_g)$, where $\bar{\mathbf{x}}=(\bar{x},z)$ is the window position at depth z and lateral location $\bar{x}$, $\bar{\theta}_s$ and $\bar{\theta}_g$ are the source and receiving angles, respectively. The LIM is a distorted estimate of the local scattering matrix (LSM) due to the acquisition aperture limitation and the propagation path effects. LSM is the intrinsic property of the scattering medium and is independent of the acquisition system and free from propagation effects and contains information of the local structure and elastic properties [20]. The task of true-reflection imaging is to restore the true LSM from the distorted LIM by applying amplitude corrections. Note that the source direction here is defined as the direction from the imaging point to the source, so it is opposite to the incident direction. The (single frequency) imaging condition in the space-local angle domain can be written as

$$L(\bar{\mathbf{x}},\bar{\theta}_s,\bar{\theta}_g)=2\sum_{\mathbf{x}_s} G_I^*(\bar{\mathbf{x}},\bar{\theta}_s;\mathbf{x}_s)\cdot\int_{A(\mathbf{x}_g)} d\mathbf{x}_g \frac{\partial G_I^*(\bar{\mathbf{x}},\bar{\theta}_g;\mathbf{x}_g)}{\partial z} u_s(\mathbf{x}_g;\mathbf{x}_s), \tag{3.2}$$

where $G_I(\bar{\mathbf{x}},\bar{\theta}_s;\mathbf{x}_s)$ is the incident wavefield in the local angle domain at the imaging point $\bar{\mathbf{x}}$ from the source at $\mathbf{x}_s$, and the integral is the back-propagated wavefield in the local angle domain from the recorded data.

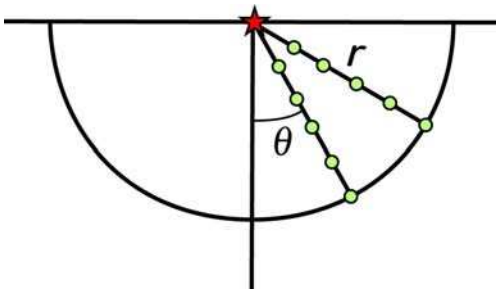

Figure 2: Diagram for extracting the amplitude along the radial direction for different angle θ. The star represents the source and the dots represent the receivers.

4 Acquisition aperture correction in the local-angle domain

Wu et al. [20] proposed an amplitude correction method in the local angle domain for the acquisition aperture correction. The relevant amplitude correction factor matrix, F_a, for above imaging condition (3.2) is

$$\left|F_a(\bar{\mathbf{x}},\bar{\theta}_s,\bar{\theta}_g)\right| = 2\sum_{\mathbf{x}_s}\left|G_I^*(\bar{\mathbf{x}},\bar{\theta}_s;\mathbf{x}_s)G_F(\bar{\mathbf{x}},\bar{\theta}_s;\mathbf{x}_s)\right|\cdot\left\{\int_{A(\mathbf{x}_g)} d\mathbf{x}_g\left|G_F(\bar{\mathbf{x}},\bar{\theta}_g;\mathbf{x}_g)\right|^2\right\}^{1/2}, \tag{4.1}$$

where G_F is the Green's function in forward modeling (for details on the amplitude correction factor, see Appendix). The final acquisition aperture corrected image can be obtained by applying the amplitude correction factor to the migration image in the local angle domain.

5 Effect of the WKBJ correction on the amplitude of the one-way propagator in smoothly varying $c(z)$ media

We will first test the effect of the WKBJ correction on the amplitude of the one-way propagator by comparing it with that from the full-wave finite-difference (FD) method. A point source is put in a smoothly varying $c(z)$ ($=3.0+0.36z$ (km/s)) medium. The source time function is a Ricker wavelet with a dominant frequency of 15Hz. To directly compare the amplitudes, we draw the curves of amplitude vs. distance from the source along radial directions for different angles θ (see Fig. 2). Fig. 3 shows the curves for angles $\theta=0^\circ,15^\circ,30^\circ,45^\circ,60^\circ,75^\circ$. Fig. 3(a) is for the conventional one-way propagator without the WKBJ correction and Fig. 3(b) is for the new propagator with the WKBJ correction. Comparison with the results from the full-wave method shows that the one-way propagator without the WKBJ correction cannot give the correct amplitudes even in smoothly varying $c(z)$ media. The larger the angle is, the larger the error of the amplitude is. For the angle $\theta=75^\circ$, a very wide angle, the amplitude obtained from the conventional one-way propagator without the WKBJ correction is only about half of the true amplitude.

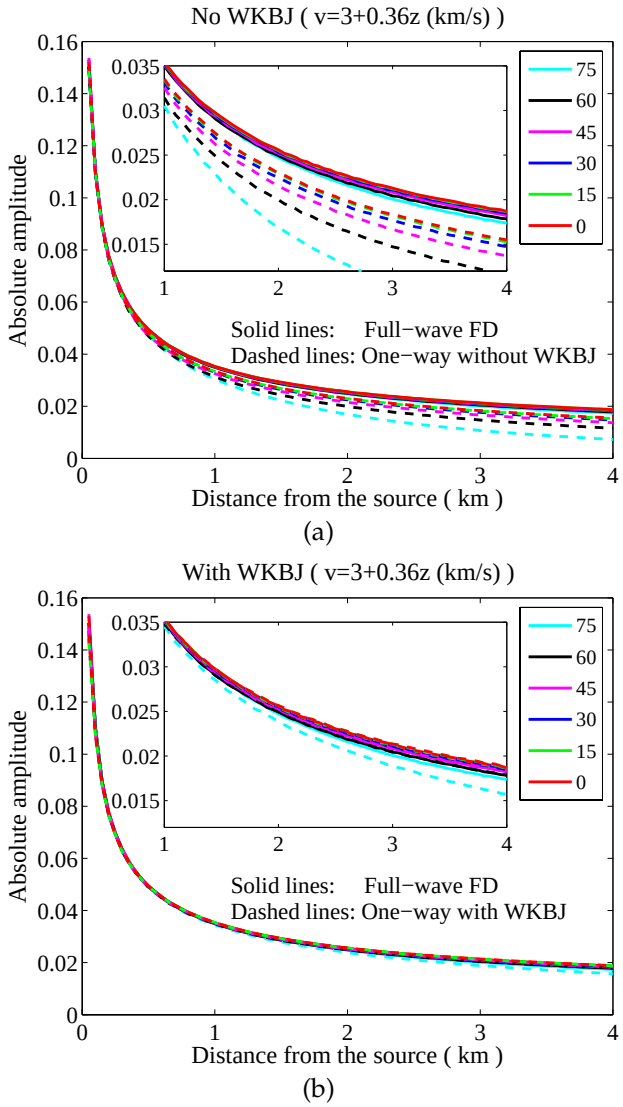

Figure 3: Effect of the WKBJ correction on the amplitudes of the one-way propagator in a smoothly varying $c(z)(=3.0+0.36z$ km/s) medium. Lines with different colors are for different angles $\theta=0°,15°,30°,45°,60°,75°$. Solid lines are results from the full-wave FD method. Dashed lines are results from the one-way method. The inset figures are zoomed in versions of the main figures. (a) is for the conventional one-way propagator without the WKBJ correction and (b) is for the new one-way propagator with the WKBJ correction.

However, with the WKBJ correction, the one-way propagator can give almost the same amplitudes as the full-wave method. Even for very large angle wave (e.g. $\theta=75°$), the difference is very small. Fig. 4 shows the seismograms obtained from the WKBJ-corrected one-way propagator and full-wave propagator along the radial direction $\theta = 60°$. The waveforms from these two methods agree very well. These demonstrate that the one-

way propagator with the WKBJ correction can give satisfactory wavefield amplitude in this smoothly varying medium. It should be noted that all of our above implementations include the contribution from evanescent waves. In our previous research [9], we found that the evanescent waves have a significant influence on the wave amplitude, especially for near-field waves.

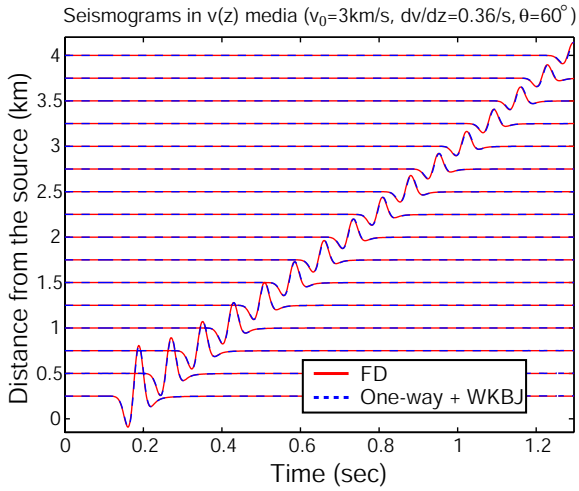

Figure 4: Seismograms obtained from the one-way propagator with the WKBJ correction (dashed blue lines) and the full-wave FD method (solid red lines) along the radial direction θ=60° in a smoothly varying $c(z)$(=3.0+0.36z km/s) medium.

6 Effect of the WKBJ correction in one-way propagators on the image amplitude

Having seen the effect of the WKBJ correction on the amplitude of one-way propagators in smoothly varying $c(z)$ media, here we will study the effect of the WKBJ correction in one-way propagators on the image amplitude in smoothly varying $c(z)$ media and also in general heterogeneous media.

6.1 Image amplitude comparison for a point scattering problem in smoothly varying $c(z)$ media

First, a simplified example is designed to illustrate the general idea in which a point scatterer is put in a smoothly varying $c(z)$ medium and the data are recorded at the surface (see Fig. 5). Theoretically, it should have the same scattering amplitude in all directions at the scattering point. To avoid possible numerical errors during generation of the dataset by directly putting the source and receivers at the surface, which may cause an anisotropic scattering pattern at the scattering point, we obtain the dataset in an indirect way. First, data are generated by a point source at the location of the point

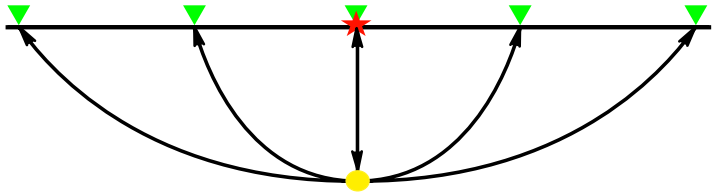

Figure 5: Diagram for the point scattering problem, in which a point scatterer (yellow dot) illuminated by a source (red star) is put in a smoothly varying $c(z)$ medium and the data are recorded by receivers (green triangles) at the surface.

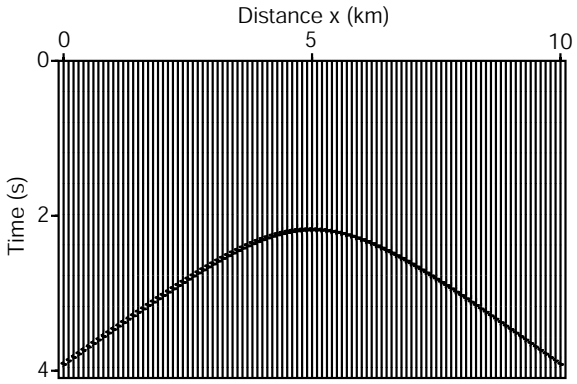

Figure 6: Single-shot data for the point scattering problem in Fig. 5. The source time function is a Ricker wavelet with a dominant frequency of 30Hz.

scatterer with the full-wave FD method and then a time delay is added corresponding to the time traveling from the real source location at the surface to the point scatterer. The velocity model used is $c(z)=1.5+0.36z$ (km/s). The receivers span an aperture of 10 km at the surface, the receiver spacing is 25 m and the source is at the center of the receiver array. The point scatterer is 2 km below the source. The source time function is a Ricker wavelet with a dominant frequency of 30Hz. The input data for the migration are shown in Fig. 6.

Because the true reflectivity (or scattering coefficient) depends on the reflection (or scattering) angle, we use the imaging condition in the local angle domain to obtain the local image matrix. Since there is only one incident angle $\theta_s=0^\circ$ for the example here, we investigate the image $L(\mathbf{x}_0,0,\bar{\theta}_g)$ at the scattering point $\mathbf{x}_0$ only in the receiving angle θ_g domain and compare it with the theoretical prediction. Fig. 7 shows the image amplitude at the scattering point in the local scattering angle domain. For the migration with the WKBJ-corrected one-way propagator and full 10 km-aperture data (solid line in Fig. 7a), the image amplitude curve within $\pm 30^\circ$ is flat, which agrees with the theoretical prediction. Without the WKBJ correction, the image amplitude (dashed line in Fig. 7a) is smaller. Results for the 6 km aperture data are similar (Fig. 7b), but the improvement after the WKBJ correction is less significant than that for the 10 km aperture data, because the WKBJ correction is more significant at wide angles.

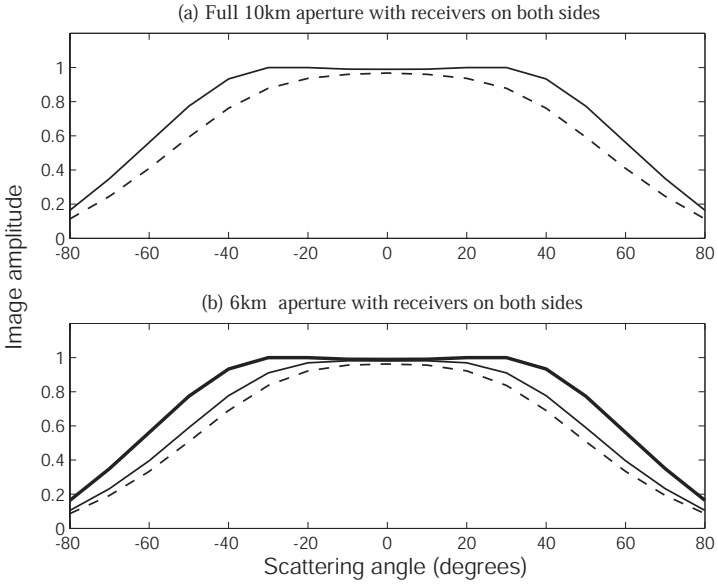

Figure 7: Comparison of the image amplitude for the WKBJ-corrected and original one-way propagators. The solid lines are the results with the WKBJ-corrected propagator, and the dashed lines are the results without the WKBJ correction. (a) Full 10km-aperture with receivers on both sides; (b) 6km-aperture with receivers on both sides (The thick solid line is the result for the full 10km-aperture with the WKBJ-corrected propagator in (a) as the reference curve).

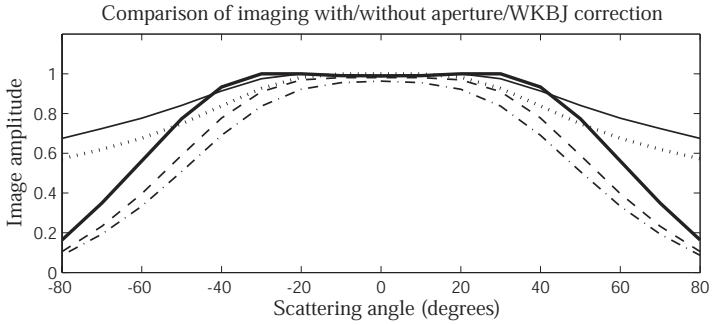

Figure 8: Comparison of the influence of the WKBJ correction and acquisition aperture correction on the image amplitude for the 6km-aperture data with receivers on both sides. Dash-dot line: original image without any correction; dotted line: result after the aperture correction only; dashed line: result with the WKBJ correction only; solid line: image with both the WKBJ and aperture correction; and the thick solid line is the result for the full-10km aperture with the WKBJ-corrected propagator as a reference curve.

From the image for 10 km and 6 km aperture data in Fig. 7b, we can see that the acquisition aperture has significant influence on the image amplitude. The acquisition aperture correction is then applied to the shorter (6 km) aperture data to minimize this effect. Fig. 8 shows that the image amplitude after aperture correction (dotted line) is significantly improved for the large scattering angle compared with that before the aperture correction (dash-dot line) for the original propagator. The aperture correction has

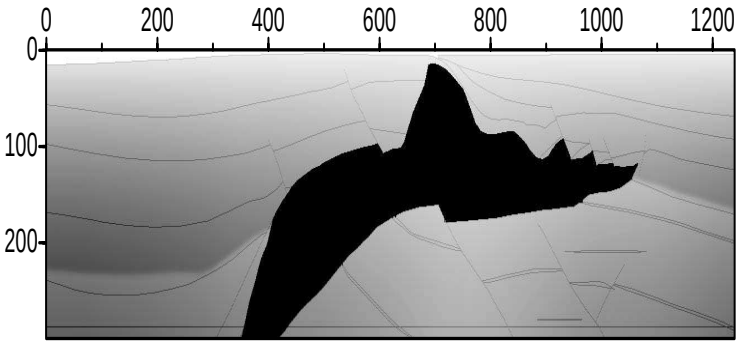

Figure 9: 2D SEG/EAGE salt model with $dx=dz=40$ feet.

a stronger effect on the image amplitude compared with the WKBJ correction (dashed line). The result with both the WKBJ and aperture corrections (solid line) gives the best amplitude distribution among them.

6.2 Image amplitude comparison for 2D SEG/EAGE salt model

In this section, we will apply the LCB beamlet propagator with the localized WKBJ correction to post- and pre-stack migration for the 2D SEG/EAGE salt model (Fig. 9) to study the influence of the localized WKBJ correction on the image amplitude.

Post-stack migration is a wave back-propagation process, which can directly show the effect of the localized WKBJ correction on the amplitude of the propagator. Fig. 10 shows the post-stack migration results before and after the localized WKBJ correction ($dx=dz=$ 40 feet). The image amplitude after correction is significantly stronger throughout the model, especially for the steep faults in the sediment, the salt boundary and the subsalt structures. The WKBJ correction also increases the amplitudes of the artifacts, especially within the salt dome and in the subsalt area.

Fig. 11 shows the pre-stack migration results ($dx=dz=80$ feet) before and after the localized WKBJ correction with the imaging condition (3.1). Similar to the post-stack case, the image amplitude is stronger throughout the model and also has stronger artifacts. To make the image amplitude after correction more closely represent the reflection strength, the image is normalized with the square of the incident wave amplitude in the local dip angle domain, which removes the dip effect from the source. The normalized images with and without the localized WKBJ correction give very similar amplitudes (Fig. 12). The small-offset acquisition (maximum offset = 14000 feet) and relatively steep dipping structures in the SEG/EAGE salt model may be the reason for the relatively weak effect of the WKBJ correction on the image amplitude. The small-offset acquisition can only acquire reflected waves with small reflection angles from the steeply dipping reflectors. The top layer is water and is laterally homogeneous. Therefore the effects of the WKBJ correction for the incident and reflected waves are similar, which makes the image amplitude improvement less significant.

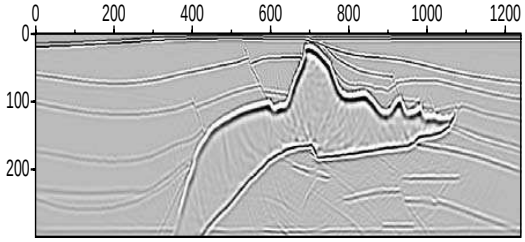

(a) Before the localized WKBJ correction

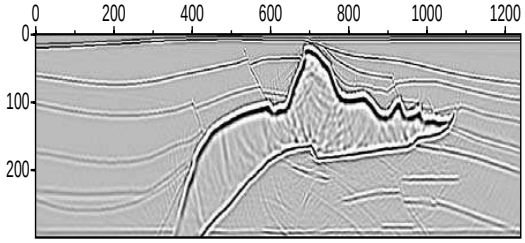

(b) After the localized WKBJ correction

Figure 10: Post-stack migration image for the 2D SEG/EAGE salt model before and after the localized WKBJ correction. Here, $dx = dz = 40$ feet.

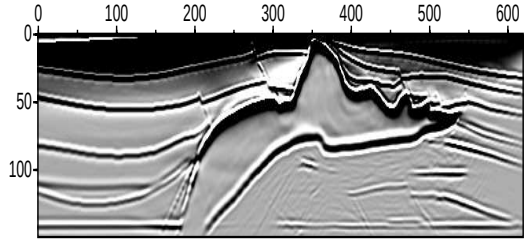

(a) Before the localized WKBJ correction

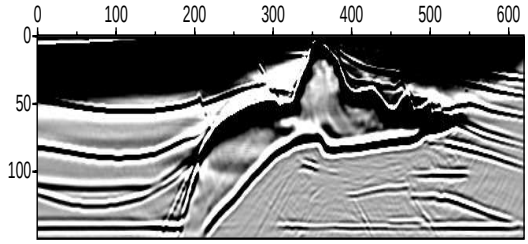

(b) After the localized WKBJ correction

Figure 11: Pre-stack image for the 2D SEG/EAGE salt model before and after the localized WKBJ correction. Here, $dx = dz = 80$ feet.

The acquisition aperture correction is also applied to the imaging. Compared with the image before the acquisition aperture correction (Fig. 11a), the image after acquisition aperture correction (Fig. 13a) is improved significantly throughout the model. The images of the steep faults in the sediment are sharper and more continuous. For sub-

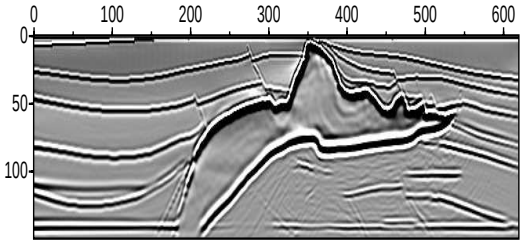

(a) Before the localized WKBJ correction

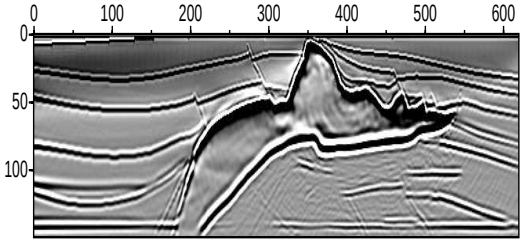

(b) After the localized WKBJ correction

Figure 12: Pre-stack image for the 2D SEG/EAGE salt model before and after the localized WKBJ correction. The image is normalized with the square of the incident wave amplitude in the dip angle domain. Here, $dx=dz=80$ feet.

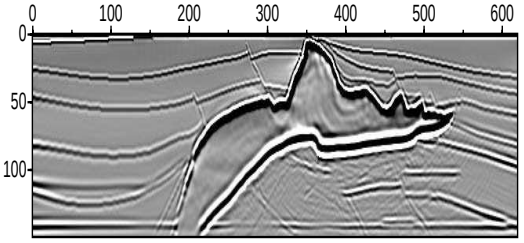

(a) Before the localized WKBJ correction

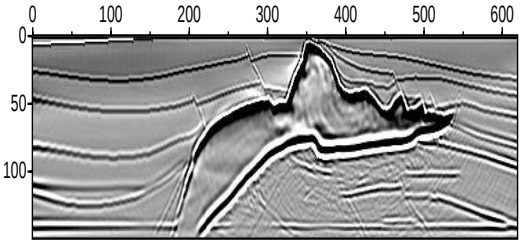

(b) After the localized WKBJ correction

Figure 13: Pre-stack image with the acquisition aperture correction for the 2D SEG/EAGE salt model before and after the localized WKBJ correction. Here, $dx=dz=80$ feet.

salt structures, the images along the steep structures and the baseline are much more uniformly distributed after the aperture correction. The artifacts in the subsalt region caused by salt body related multiples are also reduced. The result with both corrections

(Fig. 13b) shows an image similar to that with only the acquisition aperture correction, though with stronger artifacts in the subsalt area due to the WKBJ correction (Fig. 13a). These results show that the acquisition aperture correction has a stronger effect on the image amplitude for the 2D SEG/EAGE salt model. This agrees with the result for smoothly varying $c(z)$ media.

7 Conclusion

The WKBJ solution for one-way wave equations in smoothly varying $c(z)$ media is reformulated from the principle of energy flux conservation for acoustic media. Furthermore, the WKBJ solution for smoothly varying $c(z)$ media is extended to general heterogeneous media with local angle domain methods by introducing the concepts of "transparent boundary conditions" and "transparent propagators". Through numerical examples and theoretical analysis we demonstrated the following: 1. In smoothly varying $c(z)$ media the WKBJ correction for amplitudes is important to one-way wave propagators and its effect is significant for wide angle waves. 2. For seismic imaging such as depth migration, the WKBJ correction for propagators shows some improvements on image amplitudes, but not very significant. For example, the results from the 2D SEG/EAGE salt model indicate that the less-significant improvement on the image amplitude may be due to the small-offset acquisition of the data. A side-effect of the WKBJ correction in our implementation is the amplification of artifacts. 3. Comparisons between the effects of the WKBJ correction for propagators and the acquisition aperture correction show that the acquisition aperture correction has a much stronger influence on the image amplitudes, especially for the steep structures in the illumination shadow.

Acknowledgments

We greatly appreciate valuable comments and suggestions from Bjørn Ursin and another anonymous reviewer, and the guest editors Lianjie Huang and Michael Fehler. We gratefully thank Xiao-Bi Xie for helpful discussions and offering the original FD code, and thank Mingqiu Luo for helpful discussions and the help on LCB code. We also thank Alexander Hutko for proofreading the manuscript. This research is sponsored by the WTOPI (Wavelet Transform On Propagation and Imaging for seismic exploration) Research Consortium and the DOE/BES Project at University of California, Santa Cruz.

Appendix: Acquisition aperture correction in the local-angle domain

Wu et al. [20] proposed an amplitude correction method in the local angle domain for calculating the acquisition aperture correction. The imaging condition (for a single fre-

quency) in the space-angle domain to obtain the local image matrix (LIM) can be written as

$$L(\bar{\mathbf{x}},\bar{\theta}_s,\bar{\theta}_g)=2\sum_{\mathbf{x}_s}G_I^*(\bar{\mathbf{x}},\bar{\theta}_s;\mathbf{x}_s)\cdot\int_{A(\mathbf{x}_g)}d\mathbf{x}_g\frac{\partial G_I^*(\bar{\mathbf{x}},\bar{\theta}_g;\mathbf{x}_g)}{\partial z}u_s(\mathbf{x}_g;\mathbf{x}_s). \tag{A.1}$$

If there is a scatterer at $\mathbf{x}_0$ characterized by the local scattering matrix (LSM) $R(\mathbf{x}_0,\bar{\theta}_s,\bar{\theta}_g)$, the received scattered wave at $\mathbf{x}_g$ can be modeled as

$$u_s(\mathbf{x}_g,\mathbf{x}_s;\mathbf{x}_0,\bar{\theta}_s,\bar{\theta}_g)=G_F(\mathbf{x}_0,\bar{\theta}_s;\mathbf{x}_s)R(\mathbf{x}_0,\bar{\theta}_s,\bar{\theta}_g)G_F(\mathbf{x}_g,\bar{\theta}_g;\mathbf{x}_0), \tag{A.2}$$

where G_F is the forward-modeling Green's function which should be as close as possible to the point-source response (Green's function) of the acquisition process (field experiment, numerical simulations, etc.). Note that the Green's function here has been decomposed into the local angle domain at the scattering point $\mathbf{x}_0$, with $\bar{\theta}_s$ and $\bar{\theta}_g$ as the incident angle and receiving angle, respectively.

Substituting (A.2) into (A.1) we get a relation between the LIM and the LSM. The LIM is distorted from the LSM due to the acquisition aperture limitation and the propagation path effects. The task of true-reflection imaging is to restore the true LSM by amplitude corrections in the local angle-domain. The LIM and LSM are related by

$$L(\bar{\mathbf{x}},\bar{\theta}_s,\bar{\theta}_g)=F_a(\mathbf{x}_0,\bar{\mathbf{x}},\bar{\theta}_s,\bar{\theta}_g)R(\mathbf{x}_0,\bar{\theta}_s,\bar{\theta}_g), \tag{A.3}$$

where $F_a(.)$ is the amplitude correction factor for each element:

$$F_a(\mathbf{x}_0,\bar{\mathbf{x}},\bar{\theta}_s,\bar{\theta}_g)=\sum_{\mathbf{x}_s}G_I^*(\bar{\mathbf{x}},\bar{\theta}_s;\mathbf{x}_s)G_F(\mathbf{x}_0,\bar{\theta}_s;\mathbf{x}_s)B_A(\mathbf{x}_0,\bar{\theta}_g), \tag{A.4}$$

with

$$B_A(\mathbf{x}_0,\bar{\theta}_g)=2\int_{A(\mathbf{x}_g)}d\mathbf{x}_gG_F(\mathbf{x}_g,\bar{\theta}_g;\mathbf{x}_0)\frac{\partial G_I^*(\bar{\mathbf{x}},\bar{\theta}_g;\mathbf{x}_g)}{\partial z}. \tag{A.5}$$

We see that even G_F and G_I can have different dynamic behavior; however the kinematic structures of the two should be kept the same, at least to certain ranges of propagation angle (wide-angle performance). Therefore when $\bar{\mathbf{x}}$ coincides with $\mathbf{x}_0$, the image $L(.)$ in (A.3) gives a maximum value due to coherent interference. At this point, the back propagation integral represents a refocusing process for the scattered wavefield recorded by the receiver array. From an energy (amplitude) point of view, we can use a "transparent" Green's function, or precisely defined, energy-conserved Green's function G_E for back propagation. In this case, all of the energy loss that occurs during refocusing, due to boundary reflection, P-S conversion, scattering, anelastic attenuation and other effects, will be neglected. This way we can conserve all the energy collected by the receiver array to the maximum degree. This could be the best strategy for imaging and inversion since we do not want to lose any more energy from the already weak signals. Energy is conserved if we use G_E for G_I

$$|B_A(\mathbf{x}_0,\bar{\theta}_g)|^2=2\int_{A(\mathbf{x}_g)}d\mathbf{x}_g|G_F(\mathbf{x}_g,\bar{\theta}_g;\mathbf{x}_0)|^2 \tag{A.6}$$

except for some edge beamlets. By reciprocity, the beamlet Green's function in (A.6) can be calculated as radiated from a point source at $\mathbf{x}_g$ and received by a beamlet antenna at $\mathbf{x}_0$ with the same angle and beam-width. Therefore the receiver aperture effect can be simply calculated using the acquisition aperture response [21,22]. Stacking LIMs obtained from all shots, as in (A.1), we can calculate the amplitude correction factor matrix F_a,

$$F_a(\bar{\mathbf{x}},\bar{\theta}_s,\bar{\theta}_g)=\sum_{\mathbf{x}_s} G_I^*(\bar{\mathbf{x}},\bar{\theta}_s;\mathbf{x}_s)G_F(\bar{\mathbf{x}},\bar{\theta}_s;\mathbf{x}_s)B_A(\bar{\mathbf{x}},\bar{\theta}_g). \tag{A.7}$$

According to the imaging principle, the stack of the contributions from all the sources should be a coherent stack at the imaging point, resulting in

$$|F_a(\bar{\mathbf{x}},\bar{\theta}_s,\bar{\theta}_g)|=\sum_{\mathbf{x}_s} |G_I^*(\bar{\mathbf{x}},\bar{\theta}_s;\mathbf{x}_s)G_F(\bar{\mathbf{x}},\bar{\theta}_s;\mathbf{x}_s)||B_A(\bar{\mathbf{x}},\bar{\theta}_g)|. \tag{A.8}$$

References

[1] J. F. Claerbout, Coarse grid calculation of waves in inhomogeneous media with application to delineation of complicated seismic structure, Geophysics, 35 (1970), 407-418.
[2] J. F. Claerbout, Imaging the Earth's Interior, Blackwell Scientific Publications, 1985.
[3] Y. Zhang, G. Zhang and N. Bleistein, True amplitude wave equation migration arising from true amplitude one-way wave equations, Inverse Probl., 19 (2003), 1113-1138.
[4] G. Q. Zhang, System of coupled equations for upgoing and downgoing waves, Acta Math. Appl. Sinica, 16 (1993), 251-263.
[5] M. V. de Hoop, Directional decomposition of transient acoustic wave fields, Ph.D. thesis, Delft Univ. of Techology, 1992.
[6] M. V. de Hoop, Generalization of the Bremmer coupling series, J. Math. Phys., 37 (1996), 3246-3282.
[7] C. P. A. Wapenaar, Reciprocity properties of one-way propagators, Geophysics, 63 (1998), 1795-1798.
[8] D. Kiyashchenko, R.-E. Plessix, B. Kashtan and V. Troyan, Improved amplitude multi-one-way modeling method, Wave Motion, 43 (2005), 99-115.
[9] R. S. Wu and J. Cao, WKBJ solution and transparent propagators, 67th Annual International Meeting, EAGE, Extended Abstracts, 2005, pp. 167.
[10] M. Q. Luo, R. S. Wu and X. B. Xie, True amplitude one-way propagators implemented with localized corrections on beamlets, 75th Annual International Meeting, SEG, Expanded Abstracts, 2005, pp. 1966-1969.
[11] P. M. Morse and H. Feshbach, Methods of Theoretical Physics, McGraw-Hill, 1953.
[12] K. Aki and P. Richards, Quantitative Seismology, 1, W. H. Freeman and Company, 1980.
[13] R. W. Clayton and R. H. Stolt, A Born-WKBJ inversion method for acoustic reflection data, Geophysics, 46 (1981), 1559-1567.
[14] R. H. Stolt and A. K. Benson, Seismic migration: theory and practice, in: Handbook of Geophysical Exploration, Vol. 5, Geophysical Press, 1986.
[15] C. W. Frasier, Discrete time solution of plane P-SV waves in a plane layered medium, Geophysics, 35 (1970), 197-219.
[16] B. Ursin, Review of elastic and electromagnetic wave propagation in horizontally layered media, Geophysics, 48 (1983), 1063-1081.

[17] R. Burridge and H. W. Chang, Multimode, one-dimensional wave propagation in a highly discontinuous medium, Wave Motion, 11 (1989), 231-249.
[18] Y. Zhang, G. Zhang and N. Bleistein, Theory of true-amplitude one-way wave equations and true-amplitude common-shot migration, Geophysics, 70 (2005), E1-E10.
[19] D. Kiyashchenko and R.-E. Plessix, True amplitude multi-one-way modeling method: comparison of different imaging principles, 75th Annual International Meeting, SEG, Expanded Abstracts, 2005.
[20] R. S. Wu, M. Q. Luo, S. C. Chen and X. B. Xie, Acquisition aperture correction in angle-domain and true-amplitude imaging for wave equation migration, 74th Annual International Meeting, SEG, Expanded Abstracts, 2004, pp. 937-940.
[21] R. S. Wu and L. Chen, Mapping directional illumination and acquisition-aperture efficacy by beamlet propagators, 72nd Annual International Meeting, SEG, Expanded Abstracts, 2002, pp. 1352-1355.
[22] R. S. Wu and L. Chen, Directional illumination analysis using beamlet decomposition and propagation, Geophysics, 71 (2006), S147-S159.
[23] X. B. Xie and R. S. Wu, Extracting angle domain information from migrated wave field, 72nd Annual International Meeting, SEG, Expanded Abstracts, 2002, pp. 1360-1363.
[24] X. B. Xie, S. W. Jin and R. S. Wu, Wave-equation-based seismic illumination analysis, Geophysics, 71 (2006), S169-S177.
[25] R. S. Wu, Y. Wang and J. H. Gao, Beamlet migration based on local perturbation theory, 70th Annual Meeting, SEG, Expanded Abstracts, 2000, pp. 1008-1011.
[26] J. F. Claerbout, Toward a unified theory of reflector mapping, Geophysics, 36 (1971), 467-481.
[27] R. S. Wu and L. Chen, Target-oriented beamlet migration based on Gabor-Daubechies frame decomposition, Geophysics, 71 (2006), S37-S52.